Received: 30 July 2023 | Revised: 31 October 2023 | Accepted: 16 November 2023

DOI: 10.1002/hyp.15041

RESEARCH ARTICLE

WILEY

Short-term dynamics of drainage density based on a combination of channel flow state surveys and water level measurements

Izabela Bujak-Ozga[1,2] | H.J. (Ilja) van Meerveld[3] | Andrea Rinaldo[1,4] | Jana von Freyberg[1,2]

[1]Laboratory of Ecohydrology ENAC, IIE, ECHO, École Polytechinque Fédérale de Lausanne (EPFL), Lausanne, Switzerland

[2]Mountain Hydrology and Mass Movements, Swiss Federal Institute for Forest, Snow and Landscape Research (WSL), Birmensdorf, Switzerland

[3]Department of Geography, University of Zurich, Zurich, Switzerland

[4]Department of Civil, Environmental and Architectural Engineering (DICEA), Università di Padova, Padova, Italy

Correspondence
Izabela Bujak-Ozga, Laboratory of Ecohydrology ENAC, IIE, ECHO, École Polytechinque Fédérale de Lausanne (EPFL), Lausanne, Switzerland.
Email: hydrology@izabelabujak.com

Funding information
Swiss National Science Foundation, Grant/Award Number: PR00P2_185931

Abstract

Headwater streams often experience intermittent flow. Consequently, the flowing drainage network expands and contracts and the flowing drainage density (DD) varies over time. Monitoring the DD dynamics is essential to understand the processes controlling it. However, our knowledge of the event-scale DD dynamics is limited because high spatial and temporal resolution data on the DD remain sparse. Therefore, our team monitored the DD dynamics and hydrologic variables in two 5-ha headwater catchments in the Swiss pre-Alps in the summer of 2021, through mapping surveys of the flow state and a wireless streamwater level sensor network. We combined the two data sources to calculate the DD at the event-time scale. Our so-called CEASE method assumes that flow in a channel reach occurs above a set of water level thresholds, and it determined the DDs with accuracies >94%. DD responses to events differed for the two catchments, despite their proximity and similar size. DD ranged from 2.7 to 32.2 km km^{-2} in the flatter catchment (average slope: 15°). For this catchment, the discharge-DD relationship became steeper when DD exceeded 20 km km^{-2} and DD increased substantially with relatively small increases in discharge. For rainfall events during dry conditions, the discharge-DD relationship showed counterclockwise hysteresis, likely due to initially high groundwater discharge from the area near the catchment outlet; once rainfall stopped, DD remained high during the streamflow recession due to rising groundwater levels throughout the catchment. For events during wet conditions, the discharge and DD responded synchronously. In the steeper catchment (average slope: 24°), the DD varied only from 7.8 to 14.6 km km^{-2} and there was no hysteresis or threshold behaviour in the discharge-DD relationship, likely because multiple groundwater springs maintained streamflow throughout the network during the monitoring period. These results highlight the high variability in DD and its dynamics across small headwater catchments.

KEYWORDS
drainage density, IRES, non-perennial streams, rainfall-runoff events, stream network, temporary streams

1 | INTRODUCTION

In many streams, flow is intermittent and occurs only temporarily during or after rainfall or snowmelt events, resulting in an expansion of the flowing drainage network (FDN). During dry conditions, flow ceases in some channel sections, and upstream zones become disconnected from the stream network until they reconnect again during wet periods (Costigan et al., 2016). Therefore, the drainage density (DD; i.e., the total length of all flowing channels per catchment area) is variable in time (Godsey & Kirchner, 2014; Gregory & Walling, 1968).

Non-perennial rivers and streams are not only globally more prevalent than perennial ones (Messager et al., 2021), but they are also ecologically valuable (Acuña et al., 2014; Dodds et al., 2004) and provide multiple environmental services (Stubbington et al., 2020). They often host high biodiversity (Meyer et al., 2007), serve as habitats to endemic species (Stubbington et al., 2017), and as connectivity corridors (Rinaldo et al., 2018). Expansion and contraction of the FDN are vital to the persistence of aquatic species owing to the related changes in local habitat suitability (e.g., Giezendanner et al., 2021; Mari et al., 2014). The general viability of a focus species is determined by the maximum eigenvalue of a suitable landscape matrix (Hanski & Ovaskainen, 2000), which depends on the extent of the flowing network. Thus, the range of metapopulation capacities experienced by a dynamically changing flowing channel network bears key implications on our ability to predict the connection of hydrology and ecology. Moreover, intermittent streams are zones of nutrient and carbon processing (von Schiller et al., 2017). Thus, knowledge of DD is necessary to upscale CO_2 fluxes from streams (Hale & Godsey, 2019; von Schiller et al., 2017). The spatiotemporal variations of FDNs affect the hydrologic connectivity between streams and landscapes (van Meerveld et al., 2020), which can have important implications on stream biochemistry (von Schiller et al., 2017; Zimmer et al., 2022), and water management (Bertassello et al., 2022; Nikolaidis et al., 2013).

However, short-term FDN dynamics are not well documented. Most of the existing field studies investigated FDNs through walking surveys (Durighetto et al., 2020; Fritz et al., 2013; Godsey & Kirchner, 2014; González-Ferreras & Barquín, 2017; Warix et al., 2021), which is time-consuming and prone to subjectivity. Aerial surveys, for example, by drones, are not applicable in forested catchments or during precipitation events, and narrow streambeds are undistinguishable on satellite images. As a result, most data on FDN dynamics currently exist at high spatial but low temporal resolution.

To enhance the temporal resolution of FDN data, automatic sensors can be used. Flow-presence sensors are useful to automatically detect whether a channel bed is wet or dry (Jaeger & Olden, 2012; Jensen et al., 2019; Kaplan et al., 2019; Zanetti et al., 2022). However, they cannot distinguish between flowing and standing water, which can result in large uncertainties in estimating the total FDN length. The low-cost multi-sensor monitoring system of Assendelft and van Meerveld (2019) contains a flow sensor and provides more reliable data on the flowing, standing, and dry stream state. However, the high installation and maintenance efforts, especially in mountainous streams with high sediment transport rates, limit the number of sensors that can be installed and maintained and, therefore, reduce the spatial resolution of the data. Thus, sensors can provide data on FDN dynamics at high temporal resolution, but the spatial resolution remains low. Therefore, questions emerge of (1) how to combine sensor and survey data to effectively capture the short-term variations in FDN at the catchment scale, and (2) how much data are needed to reliably monitor FDN variations.

Because of the difficulties in capturing short-term FDN dynamics by field observations, some recent research efforts focused on developing modelling frameworks that simulate FDN expansion and contraction. Ward et al. (2018) and Mahoney et al. (2023) used physically-based modelling approaches, whereas Senatore et al. (2021) used topographic and geological data to model network dynamics. Kaplan et al. (2019) used a random forest model to identify the temporally changing factors that explain streamflow responses in intermittent streams at the event scale, with predictors including precipitation, soil moisture, and temperature. Botter et al. (2021) described the concept of hierarchal activation of drainage networks, which were later used to develop a simple analytical model (Durighetto & Botter, 2022) and a more complex stochastic model (Durighetto, Bertassello, & Botter, 2022; Durighetto, Mariotto, et al., 2022) of FDN dynamics. Recently, Aho et al. (2023) used directed acyclic graphs to summarize and track non-perennial stream characteristics as FDN expand and contract. However, all these FDN modelling studies face challenges of limited FDN training data. They have not yet been applied extensively in different catchment settings, hindering inter-catchment comparisons and, as a result, limiting our understanding of the variability of the processes controlling FDNs.

Because FDNs reflect the underlying hydrological processes (Shanafield et al., 2021), monitoring FDNs together with other hydrological variables can lead to a better understanding of runoff processes. Godsey and Kirchner (2014) proposed that the time and position of flow occurrence along a drainage network reflects the balance between water transport from the upstream reach and subsurface transmissivity. Therefore, the FDN dynamics may offer important clues to the spatial structure of the hyporheic zone and streamflow generation mechanisms. For example, Warix et al. (2021) found that streams in a semi-arid catchment dried out when contributions from shallow flow paths were low and that there was a high surface flow persistency for streams with seasonal stable groundwater inputs. Similarly, Zimmer and McGlynn (2017a, 2017b) showed that catchment storage variations affected streamwater-groundwater interactions and flow permanence

in a 0.033 km^2 catchment in the Piedmont region of North Carolina, USA. The system alternated between a losing stream with rainfall-induced onsets of flow and a gaining stream with continuous flow during low- and high-catchment storage, respectively. Although there were distinct groundwater flow paths during low and high catchment storage states, the relationship between FDN length and stream discharge was persistent (Zimmer & McGlynn, 2017c). These studies highlight the benefit of analysing FDN dynamics together with other hydrological variables to better understand hydrological processes in highly dynamic headwater catchments.

In this study, we investigate DDs variations in two small pre-Alpine headwater catchments at high spatial and temporal resolution. Our work is structured around two sets of research questions that focus on the methodological aspects of estimating DD variations (question 1 and 2), and the hydrological processes that lead to DD variations (question 3 and 4). Specifically, we want to know:

1. How can we combine surveys and continuous water level data to determine DD variations at a high spatial and temporal resolution?
2. How much data do we need to properly estimate short-term DD variations?
3. How variable are the DDs in our study catchments across time and space?
4. How are short-term DD dynamics related to catchment water storage and what can we learn from these relationships about streamflow generation in our study catchments?

2 | METHODOLOGY

2.1 | Study sites

2.1.1 | Location and topography

This study was carried out in two sub-catchments of the pre-Alpine Erlenbach research catchment (Staehli et al., 2021; Figure 1): Langried (Lan) and Chaspersböden (Cha). The Erlenbach catchment (Erl) has an area of 0.7 km^2 and ranges in elevation from 1080 to 1520 m a.s.l. The outlets of the two sub-catchments are located 1.3 km from each other. The Erl catchment has a westerly aspect and is locally steep. The 0.048km^2 Langried (Lan) sub-catchment ranges from 1292 to 1244 m a.s.l., has an average slope of 15°, and is representative of the lower and flatter part of the Erl catchment. The 0.043 km^2 Chaspersböden (Cha) catchment, ranges from 1552 to 1656 m a.s.l., has an average slope of 24°, and represents the steeper spring zone of the Erl catchment. The springs occur at the break in slope (average slope below the springs of 15° vs. 27° for the hillslopes above the springs; see Figure 1). The break in slope is likely caused by a fault zone and change in the Flysch bedrock.

As a consequence, the channel network in Cha is concentrated in the flatter part of the catchment, whereas in Lan the channel network extends across the entire catchment. The width of the channel reaches ranged from ca.10 cm at channel heads to 50 cm at catchment outlets; most of the main channel reaches were ca. 20–30 wide.

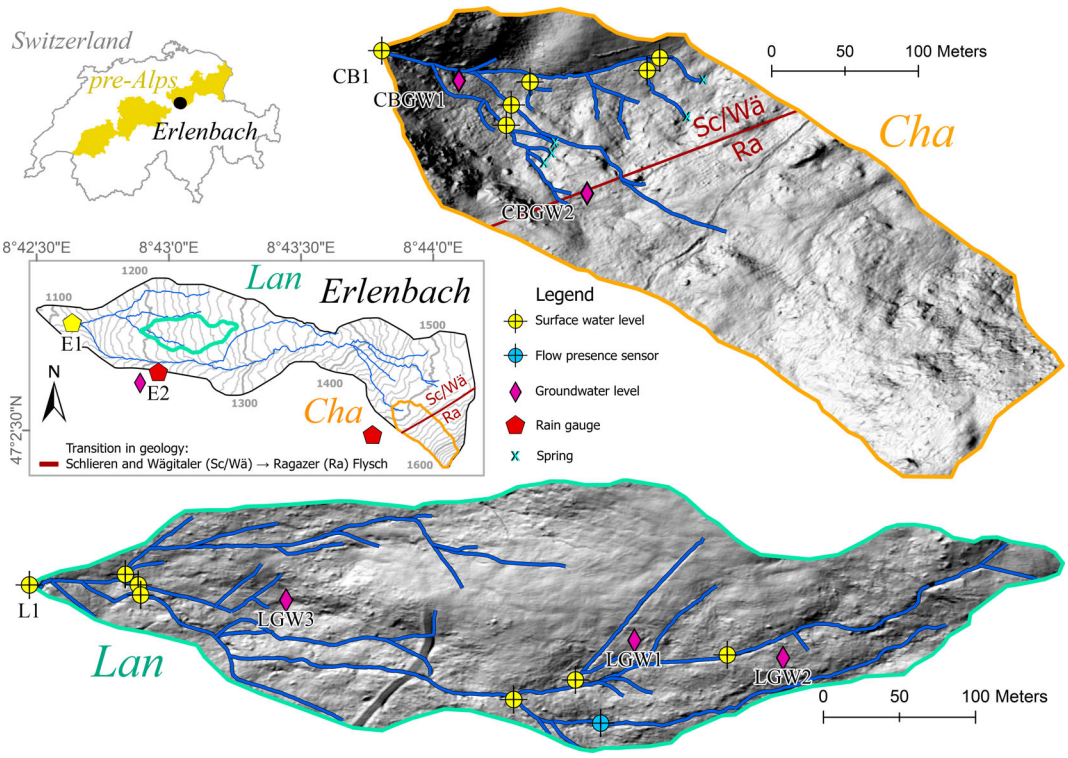

FIGURE 1 Map of the study site and monitoring network. The insets show the location of the Erlenbach catchment and the pre-Alps in Switzerland and the location of the Cha (orange) and Lan (b) in the Erlenbach catchment. The coordinate system is CH1903/LV03. The hillshade map is based on the digital elevation model with a 0.5 m resolution (swissALTI3D, SwissTopo); border between Schlieren and Wägitaler Flisch and Ragazer Flisch is based on Geological Map of Switzerland 1:500 000 (GK500; SwissTopo).

The topographic wetness index (TWI; Beven & Kirkby, 1979), based on the 0.5 m resolution digital elevation model (swissALTI3D; SwissTopo - Federal Office of Topography swisstopo, 2019), is higher (6–9) close to catchments outlets and along main streams than for the remaining catchment areas (0–5).

2.1.2 | Climate

The average annual precipitation at 1210 m a.s.l. in the Erl catchment is 2266 mm (water years 1969–2019; Staehli et al., 2021). Snowfall represents a third of the total precipitation. A continuous snow cover of up to 2 m thick can be present from December to April (von Freyberg et al., 2022). The mean monthly temperature varies from −1.9 to 15.9°C (von Freyberg et al., 2022). The 2021 summer study period was relatively wet, especially in July. Total precipitation at the rain gauge close to the Lan (Figure 1) in July 2021 was 548 mm month^{-1}; between 2010 and 2020, it ranged from 77 to 530 mm month^{-1}.

2.1.3 | Land-use, geology, and pedology

The Lan catchment is characterized by forests, grasslands and wet meadows. The coniferous forests are dominated by Norway spruce (*Picea abies*) and silver fir (*Abies alba*) (Staehli et al., 2021). The catchment is located on Wägitaler and Schlieren Flysch bedrock. The wet meadows in the Lan catchment are located on Holocene deposits interspersed by Pleistocene moraine (till) deposits (Hantke et al., 2022). In Lan, a few channels are artificial ditches.

The Cha catchment is mainly covered by grasslands and wet meadows (lower part), with isolated groves of trees. The catchment is used for cattle grazing in summer. The Cha catchment is underlain by Ragazer Flysch (upper hillslope) and wet meadows on Holocene deposits in the lower parts (Hantke et al., 2022). In Cha, there are no artificial alterations to the drainage network. Shallow and low-permeability gleysols throughout the Erl catchment lead to shallow groundwater tables in large parts of the catchments for most of the year (Rinderer et al., 2014).

2.2 | Field measurements

2.2.1 | Hydrometric measurements and data

We used air pressure and temperature compensated pressure transducers (CTD10, Meta, Pullman, USA) and pressure transmitters (26Y, Keller AG, Winterthur, Switzerland) to continuously monitor stream water levels at seven locations in Lan and six locations in Cha (Figure 1). The pressure transmitters were placed in the middle of the channel cross-sections. In Lan, water level data at 5-min resolution are available from the 1st of June to the 27th of October 2021 (except for LGW3, which was added on the 9th of September 2021). In Cha, water level data at a 5-min resolution are available from the 18th of June to the 27th of October 2021 (except for CB1, which was added on the 1st of June 2021). In both catchments data gaps of up to a few hours occurred sporadically due to data transmission errors and measurement disturbances, for example, during water sample collection.

Discharge time series were determined from water level measurements behind V-notch weirs using the Kindsvater-Shen equation (Kulin & Compton, 1975), which was checked using 32 and 26 bucket measurements at a range of low to medium flow rates in Lan and Cha, respectively. Water level and discharge data from the WSL gauging station above the sedimentation basin for the Erl catchment (E1; Figure 1) were provided by WSL's Mountain Hydrology and Mass Movements research unit. Water levels were measured at this location using pressure transducers and recorded by digital Philips and Campbell dataloggers. The stage-discharge relationship was obtained by salt-dilution measurements (Staehli et al., 2021).

Groundwater monitoring tubes (PVC; screened at an interval of ca. 1 cm over the lowest 50 cm) were installed 5–11 m from the nearest channel at depths of 1.19–1.44 m below the soil surface (Figure 1). Soil moisture sensors (Terros 12, Meter Group, Pullman USA) were installed at three different depths (10, 30, and 50 cm) near the groundwater monitoring tubes. Precipitation was monitored at a 10 min resolution using tipping bucket rain gauge at 1502 m a.s.l. near the Cha catchment (Figure 1; DL-TBRG-001, Decentlab, Switzerland). Precipitation data at a 10 min resolution at 1210 m a.s.l. at the Erlenhöhe climate station near Lan (Figure 1; Pluvio2 L400 RH, Ott Hydromet GmbH, Switzerland) were provided by WSL's Mountain Hydrology and Mass Movements research unit.

2.2.2 | Channel mapping

First, we mapped the complete channel networks in the Lan and Cha catchments. We define a channel as a depression or landscape feature where directed surface flow occurs or where there are visible signs that flow occurred in the past (e.g., flattened grass along the flowpath after rainfall). The total length of all channels (both flowing and dry) was 1939 m, and 742 m in Lan and Cha, respectively. Longer channels were divided into shorter reaches (Figure S1 and Figure S2) and their start and end points were defined based on the observed similarity in the hydrologic conditions.

Between the 1st of June and the 27th of October 2021, we mapped a total of 85 and 48 reaches during 15, and 14 surveys in Lan and Cha, respectively. We timed the surveys to capture a wide range of hydrologic conditions. During each survey, a person walked along the entire drainage network and classified all channel reaches within a sub-catchment as either 'flowing' when there was any directed surface flow in the reach, or 'not flowing' when the flow was absent. 'Flowing' reaches were subdivided into flowing (>5.0 L min^{-1}), weakly flowing (2.0–5.0 L min^{-1}), trickling (1.0–2.0 L min^{-1}), or weakly trickling (0.01–1.0 L min^{-1}). 'Not flowing' reaches were further categorized into 'standing water', 'wet streambed', or 'dry streambed'.

These seven categories helped in understanding the spatial variation of the flow regime and achieving the reproducibility of the surveys. Each survey was conducted within a few hours. Besides these regular catchment-wide surveys, we recorded individual visual observations of the channel states at selected reaches during equipment maintenance. We used the TempAqua App iOS (Bujak-Ozga, 2023a) to gather all georeferenced measurements, photos, and videos in the field. In one ephemeral tributary (Figure 1), visual observations of reach states were complemented with measurements from a flow sensor (Assendelft & van Meerveld, 2019). Because this sensor only registered flow larger than approximately 1 L min^{-1}, we used only the data when the sensor registered flow to assure congruence with the surveys.

2.3 | Calculation of drainage density time series with the CEASE method

2.3.1 | The CEASE method

We define the DD as the total length of all channel reaches with visible directed surface flow per unit of drainage area (Horton, 1932). To determine the DD response to rainfall events in Lan and Cha, we combined the high temporal resolution water level time series with the high spatial resolution surveys. More specifically, we calculated the 10-min DD time series as follows:

$$DD(t) = \frac{1}{A} \cdot \sum_{i=1}^{n} S_i(t) \cdot L_i \quad (1)$$

Where $DD(t)$ is drainage density at the time t, A is the catchment area, $S_i(t)$ is a predicted binary of the state of channel reach i at time t (0 for 'dry' or 1 for 'flowing'), and L_i is the length of the reach i. The calculated $DD(t)$, thus, does not differentiate between connected and disconnected flowing channel reaches.

To predict $S_i(t)$, we developed a method that relates S_i to the measured water levels. We refer to this method as the CEASE (ConsEnsuAl State Estimation) method. The CEASE method conceptually follows the Random Forest Classifier (Ho, 1995) and is derived from the idea that predictions made by many models together will outperform individual constituent models.

Equation (2) shows the function $S_i(t)$ that returns a binary value, 1 when the state of the channel reach i is predicted as flowing or 0 when dry:

$$S_i(t) = \begin{cases} 0, & \sum_{j=1}^{J} V_{ij}(t) < \frac{J}{2} \\ 1, & \text{otherwise} \end{cases} \quad (2)$$

where $V_{ij}(t)$ is a vote, that is, the state of the channel reach i predicted using water level data from sensor j at the time t, and J is the total number of sensors that are used to make the prediction. The vote $V_{ij}(t)$ returns a binary value, following Equation (3):

$$V_{ij}(t) = \begin{cases} 0, & W_j(t) < T_{ij} \\ 1, & \text{otherwise} \end{cases} \quad (3)$$

where $W_j(t)$ is the water level measured by sensor j at the time t, and T_{ij} is a classification threshold for channel reach i and sensor j. This classification threshold was calculated (i.e., optimized) to achieve the highest prediction accuracy.

In Figure 2, we schematically present the calculation of the classification threshold T_{ij} and the CEASE method. The input data consists of water level time series collected at multiple locations (step 1 in Figure 2, and section 2.2) and visual observations of channel states along the network from surveys (step 2 in Figure 2 and section 2.2). Firstly, we combined the visual observations of a channel reach i at times t with the water level measured by a sensor at that time (±5 min) (step 3.1 in Figure 2). Secondly, we determined the thresholds T_{ij} (step 3.2 in Figure 2) above which the stream reach was flowing and below which it was not. Thus, we classified the state of channel reach i as 'flowing' when the water level registered by sensor j exceeded the threshold T_{ij} and as 'no flow' otherwise (step 3.3 in Figure 2, Equation 3). Technically this was done by implementing the receiver operating characteristic (ROC) curve algorithm. Hereby, we determined the number of correctly classified states for all possible threshold values and choose the threshold that results in the best performance. If multiple thresholds had a similar performance, then the average value was chosen. We repeated this classification for each sensor and then compared the J predictions of the state of reach i and chose the state that was predicted by the majority of the sensors (i.e., consensus) as the final prediction of the channel state for reach i for that timestep (step 3.4 in Figure 2, Equation 2). In the rare cases that a draw occurred, we excluded the sensor with the most uncertain threshold estimate from the analysis. The threshold estimation for reach i was considered most uncertain when the difference between T_{ij} and the closest water level measured by sensor j during 'flow', or 'no-flow' observations was larger than for all other sensors (Figure 2, 3.2).

We repeated these steps for each channel reach i (step 4 in Figure 2), and thus created a time series of 'flow'—'no flow' for each reach in the catchment. The DD time series for the entire catchment was then obtained from the total length of all 'flowing' reaches (Equation 1). The flow persistency of a reach was calculated based on the 10-min CEASE method estimates as a percentage of the time that the reach was flowing. We did all calculations in R software (R Core Team, 2022).

2.3.2 | Method performance

The performance of the CEASE method was assessed based on the accuracy, sensitivity, and specificity. Accuracy represents the number of correctly identified reach states (flowing, not flowing) divided by the total number of assessments. Sensitivity was defined as the number of correctly identified flowing reach states divided by the number of all identified flowing reach states. Finally, specificity represents the

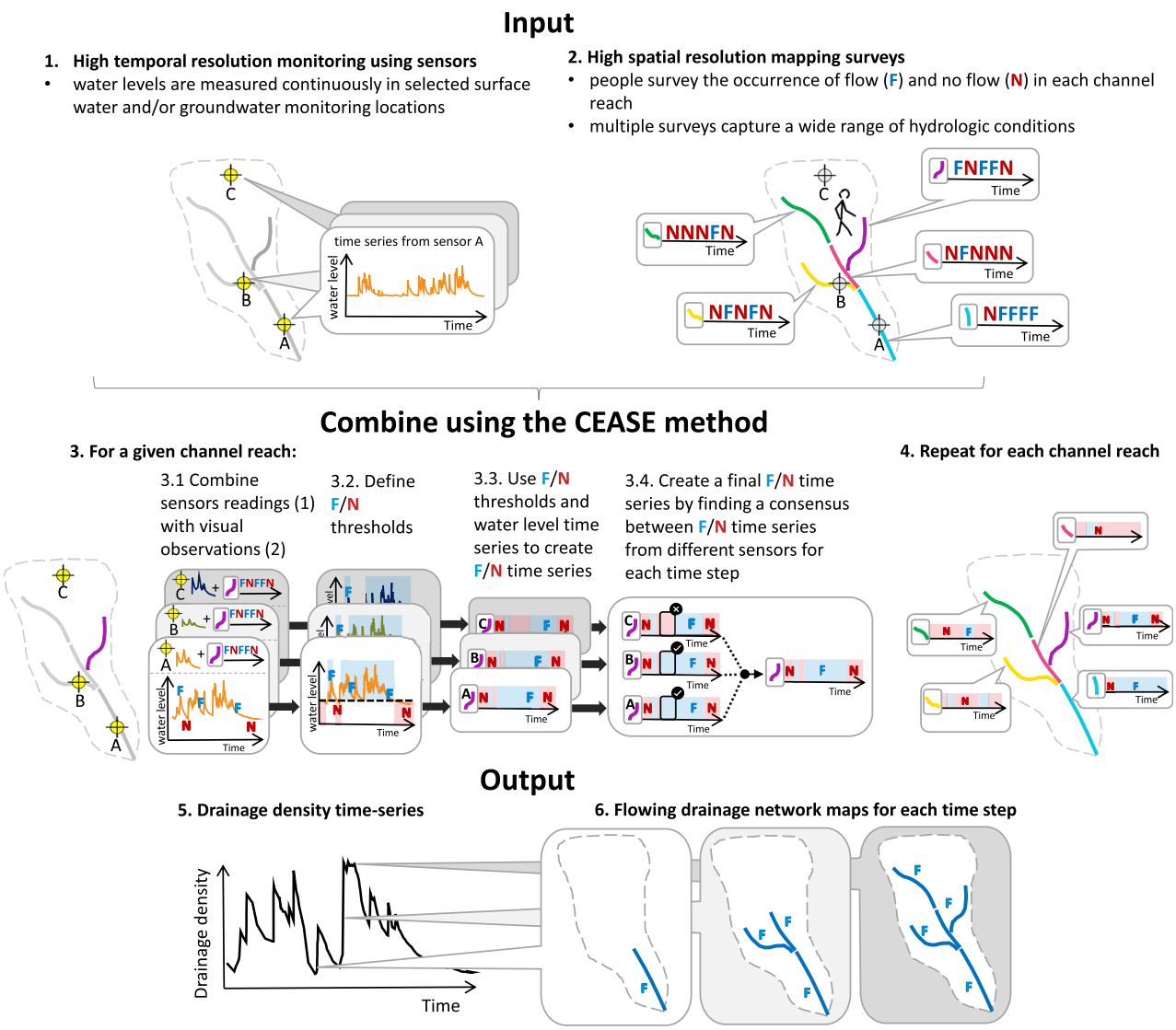

FIGURE 2 Schematic explanation of the CEASE method to derive the drainage density (DD) from high-resolution water level time series at a few points across the catchment (1) and repeated high spatial resolution surveys of the flow state throughout the catchment (2). For each channel reach (example highlighted in purple in (3)) the mapped time series of flow (F) and no-flow (N) is compared to the measured water levels at a water level monitoring location to determine the water level threshold above which flow occurs (3.2). Based on this threshold the water level time series is converted to a flow/no-flow time series for the reach (3.3). This comparison is repeated for all water level monitoring locations (3.1–3.3), regardless of their distance to the reach. Finally, for each time step the flow or no-flow estimates from the sensors are compared and the majority (i.e., consensus) is used to determine the flow state of the reach (3.4). These steps (3.1–3.4) are repeated for all reaches (4) to obtain maps of flow or no-flow for every reach (6) and the DD for each time step (5).

number of correctly identified not-flowing reach states divided by the number of all identified not-flowing reach states.

2.3.3 | Identification of the optimal data set to determine the flow state

We used cross-validation to identify the most informative data set to determine the DD time series and to gain further insights into the performance of the CEASE method when different input datasets are used. We divided our data into an input (training) dataset for the calculation of T_{ij} and a dataset for method performance evaluation (validation).

To evaluate the importance of the different water level monitoring locations for the determination of the DD, we varied the type (surface water or groundwater) and the number of monitoring sites (all available surface water sensors or outlet only) used as input for the calculation of the T_{ij} thresholds. This resulted in four different tests for which we used all available visual observations (1451 and 740 flow state observations for Lan and Cha, respectively).

To assess the number of surveys required to robustly determine the DD in combination with the high temporal resolution water level

data, we performed a leave-*p*-out cross-validation, where we used only selected surveys together with all available surface water and groundwater level (GWL) data from the sensors as input. In each test, we left a *p* number of surveys, ranging from one to *N*-1, out of the input dataset and repeated the test *N* times. Here, *N* is the total number of surveys available for a catchment (i.e., 15 for Lan and 14 for Cha). For each test, we selected the surveys randomly, without repetition. The validation dataset consisted of all surveys not used as input, that is, *N*-*p*.

To evaluate the role of hydrological conditions during the surveys on the performance of the CEASE method, we performed three tests representing the dry, wet, and entire range of hydrological conditions. For each of the three tests, we selected three surveys representative of the respective conditions, specifically, surveys with the largest, smallest, and variable (max, min, and median value) DD. The validation dataset consisted of all (*N*-3) other surveys.

For comparison, we performed an additional evaluation for the best-case scenario using all water level sensor data from all surface water and GWL monitoring locations, as well as all survey data for input and validation. Moreover, we calculated the performance metrics for the best-case scenario without the measurements at the catchment outlet because we used these results to evaluate the relation between DD and discharge (see sections 3.2 and 3.3).

2.4 | Event definition

Based on the discharge and precipitation time series, we distinguished 27 rainfall events during the monitoring period (Figure S8). We defined the beginning of a rainfall event as the onset of precipitation that resulted in a substantial increase (>150%) in discharge, and the end of an event as the time that discharge returned to its pre-event level or the start of the next event. We defined the antecedent wetness conditions as those when both discharge and GWLs were low. Specifically, we classified events as those with dry antecedent conditions when the average discharge at L1 was <4.5 L min^{-1} in the 2 days prior to the event. This threshold was selected because it also includes all events occurring after longer periods with low GWLs (i.e., average water level <−142 cm at location E2 in the 2 days prior to the event).

3 | RESULTS

3.1 | Conditions and DD dynamics during the monitoring period

There were two distinct hydrological periods during the 5-month study period: wet conditions with frequent intense rainfall events from June to mid-August 2021, and drier conditions with less frequent and lower intensity rainfall after mid-August 2021 (Figure 3). In the first period, the GWLs remained high. In the drier period, GWLs decreased more between rainfall events (Figure 3 and Figure S3), due to the lower and less frequent precipitation and higher evapotranspiration.

The surveys covered a wide range of flow conditions (Figure 4). Only a minor part of the channel network in the two catchments remained non-flowing during all surveys (Figure 3c); the smallest surveyed DD was 2.7 and 7.8 km km^{-2} for Lan and Cha, respectively; the largest possible DDs were 40.0 and 15.2 km km^{-2} for Lan and Cha, respectively. The DD dynamics differed considerably for the two catchments (Figure 3c): in the wet period, DD in Lan reacted dynamically to rainfall events, shifting between minimal and maximum DD values within 15 min. In contrast, the absolute DD variations in Cha were much smaller because the DD was mostly at or close to its maximum value. In the dry period, DDs increased dynamically after rainfall events in both catchments, again at time scales of around 15 min. However, the maximum DDs occurred less frequently in Lan and Cha.

3.2 | Evaluation of the CEASE method

When the CEASE method was used with all water level data, all calculated performance metrics were high (>80%; Table 1). The simulated DDs obtained with this best-case scenario agree well with the mapping surveys (average of DDs calculated between mapping survey start and end) for both Lan ($R^2 = 0.96$, $p < 0.01$) and Cha ($R^2 = 0.75$, $p < 0.01$).

When the data from only one sensor data set was used in the CEASE method, the differences in the method performance metrics were negligible. The largest effects occurred for the specificity for Cha, which ranged from 79% (only surface water level data from the Cha outlet) to 90% (only GWL data). All other performance metrics were higher than 94%, regardless of the sensor dataset that was used as input for the CEASE method.

When three or fewer surveys were used, the performance metrics were substantially lower on average and had a higher standard deviation for Lan. When at least six surveys were used as input, the performance metrics were relatively stable, averaging around 90%, 85%, and 92% for accuracy, sensitivity, and specificity, respectively (Figure 5a,c,e). For Cha, the average specificity and accuracy were also lower and had a higher standard deviation when three or fewer surveys were used; they became stable when at least five surveys were used (Figure 5b,d). The standard deviation of the accuracy was small standard deviation (<10%) for Cha but for the specificity it was higher (>20%). Sensitivity stayed above 90% for all tests (Figure 5f).

When only the three surveys during dry conditions were used the accuracy of the simulated DDs was lower than when three surveys during varying conditions were used as input data by 25% and 5% for Lan and Cha, respectively (Table 1). The lower accuracy was associated with a lower sensitivity; specificity remained above 82% for both catchments. When only the three wettest surveys were used as input, both the accuracy and specificity decreased substantially, whereas sensitivity was above 96% for both catchments.

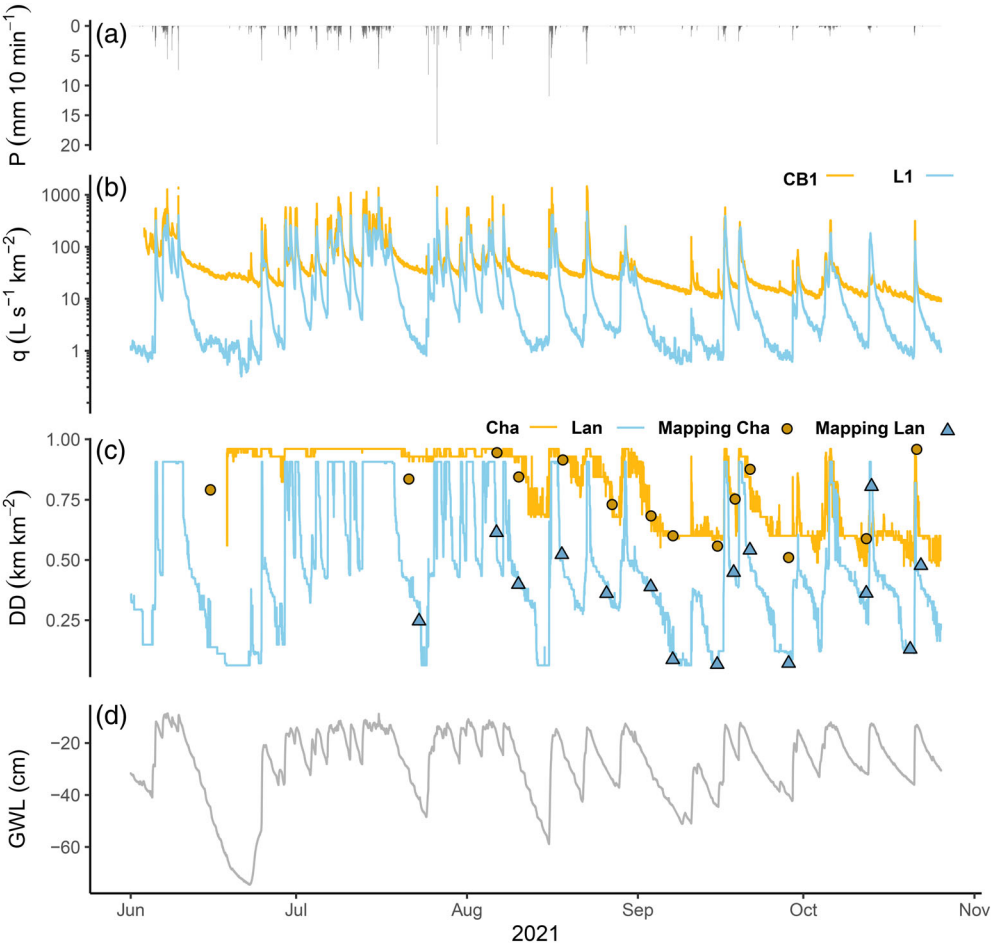

FIGURE 3 Time series of precipitation measured close to Lan (a), specific discharge (Lan in blue and Cha in orange) (b), drainage density DD (surveys: symbols, CEASE method: lines) (c), and groundwater level at location LGW1 (d) during the study period. The drainage density was calculated with the CEASE method, using all stream and groundwater level sensor data (except for the catchment outlets) and all visual observations of the channel states. For readability of the figure only the groundwater level at LGW1 is shown; the groundwater levels measured at all locations are shown in Figure S3.

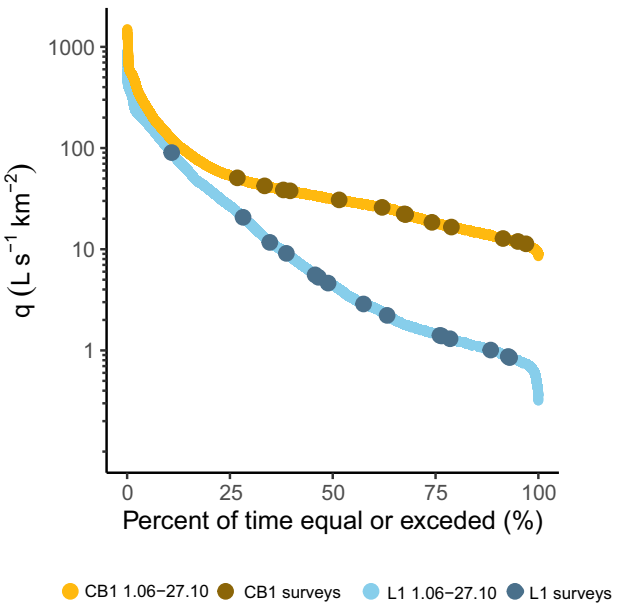

FIGURE 4 Flow duration curves for discharge measured at L1 (the outlet of Lan catchment) and CB1 (Cha catchment) in yellow, and blue, respectively. Dots in darker colours mark the discharge at the times of the mapping surveys. Dots in lighter colours mark the discharge measured throughout the study period.

3.3 | Relationship between DD and specific discharge

The relation between the 10-min data of the simulated DD and the specific runoff is very different for the two catchments (Figure 6). In Lan, the slope of the DD-q relationship is steep until DD is around 15 km km^{-2}, and then flattens for mid-range discharge values and a DD between 15 and 20 km km^{-2}. At high flows of around 20 Ls^{-1} km^{-2} and DDs higher than around 20 km km^{-2}, the relationship becomes steep again until the maximum DD is reached. In contrast, the range of the DD-q relationship for Cha is much smaller and its slope is similar to that for the high-flow conditions in Lan (Figure 6).

To identify which parts of the catchments contribute to streamflow, we investigated the spatial patterns in flow persistency and related them to the DD-q plot (Figure 7). The Lan main stream has a flow persistency of 100% (i.e., was always flowing), whereas the least incised (<10 cm) reaches below the channel heads and artificial ditches have the lowest flow persistencies (Figure 7a). The steep DD-q relationship in Lan when the DD was <15 km km^{-2} can be explained by the stream network expanding along the main tributaries that have a flow persistency >70%. For some of these tributaries, the downstream reaches were sometimes activated later than the upstream ones. For

TABLE 1 Accuracy, sensitivity, and specificity (in %) for the drainage density for the Lan and Cha catchments calculated with the CEASE method with different input data. GW, SW, and E1 stand for all groundwater level sensors, all surface water level sensors, and the water level at the Erlenbach outlet, respectively.

	Scenario	Best-case		Different sensors				Different surveys		
	Sensors used	All	All but outlet	GW	SW	Outlet	E1	All	All	All
	Surveys used	All	All	All	All	All	All	Wet	Varying	Dry
Accuracy	Lan	96.2	95.8	95.7	95.5	94.8	94.1	76.2	87.6	62.7
	Cha	93.6	94.5	96.4	92.6	92.7	95.8	82.1	84.3	79.8
Sensitivity	Lan	95.6	95.6	94.5	95.0	95.1	94.2	96.2	76.5	31.4
	Cha	96.7	96.8	98.0	95.3	95.8	97.7	98.7	84.7	77.2
Specificity	Lan	96.7	96.0	96.6	95.8	94.6	94.1	62.9	96.7	97.2
	Cha	80.6	84.8	89.7	80.6	79.1	87.8	24.1	82.7	96.3

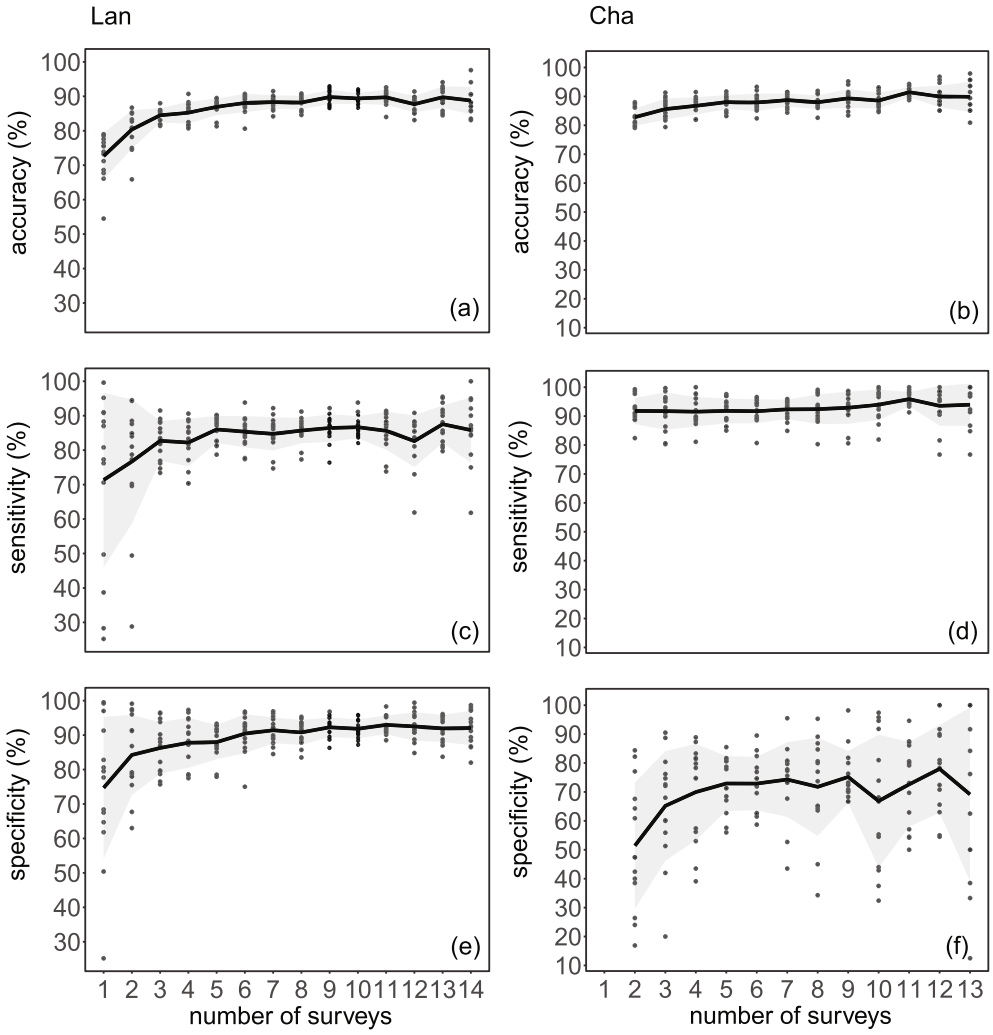

FIGURE 5 Performance metrics, accuracy (a, b), sensitivity (c, d), and specificity (e, f) of the CEASE method for the estimated channel states in Lan (left) and Cha (right) when a different number of surveys were used as the input (leave-p-out cross-validation). The black line represents the average value for a given number of surveys. Shaded areas represent one standard deviation. For Cha, the test with one survey is not shown because gaps in the water level data caused the performance metrics to be incomparable.

DD between 15 and 20 km km^{-2}, the stream network expanded into tributaries with more incised stream channels and into the upper parts of the main tributaries, both having flow persistencies between 25% and 70%. The DD-q relationship steepens again for DD >20 km km^{-2} when shallow-incised channels near the channel heads and ditches began to flow (persistencies ≤25%, Figure 7a).

In Cha, the main-stream and tributaries with a flow persistency of 100% accounted for 49% of the total drainage network length (Figure 7b). The moderately incised, smaller uphill tributaries had flow persistencies between 50% and 70%. In only 7% of the network, mainly located downstream of the two southern channel heads, flow occurred for ≤30% of the time (Figure 7).

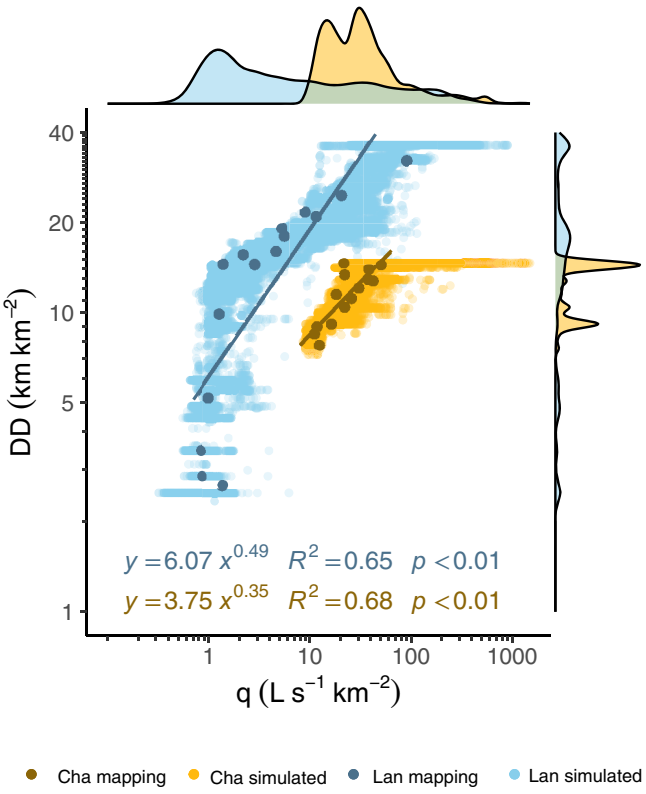

FIGURE 6 The relationship between drainage density (DD) and specific discharge in Lan (blue) and Cha (red). The darker colours represent the data from the surveys, the lighter colours the 10-min resolution results from the CEASE method when all data were used as input. Regression lines were fitted to the data from the surveys for illustrative purposes; R^2 values and best-fit equation are shown in the graph. The frequency distributions of the specific discharge and simulated DD are shown outside the axes.

3.4 | Dynamics of DD and hydrological variables during rainfall-runoff events

The simulated 10-min DD time series allows us to study the processes that govern the FDN dynamics during rainfall events. As an example, five rainfall events in Lan are shown in Figure 8. For the events on the 22nd and 24th of June, after dry antecedent conditions, the DD-q relationships exhibited a counter-clockwise hysteresis, although specific discharge and DD peaked at the same time (Figure 8d). For events following wetter antecedent conditions (i.e., the events on the 3rd and 6th of July), there is almost no visible hysteresis (Figure 8d). Furthermore, the DD-q relationships during the hydrograph recessions were less steep for the events after dry conditions than for the events with wet antecedent conditions.

When comparing DD and GWL, which is used here as a proxy for subsurface water storage, we see clockwise hysteresis for the events following dry antecedent conditions (e.g., on June 24th; Figure 8e and S4), except that there was no clear hysteresis for the driest conditions (22nd of June). Instead, groundwater level increased during both the rising limb and recession phase of this event. DD peaked earlier and decreased faster than the GWL. DD and GWL responded simultaneously for events for which the GWL at the start of the event was within 35 cm from the surface (e.g., for the events on July 3rd, 6th, and 10th). For all events, there was a noticeable change in the slope in the DD-GWL relationship when the GWL rose to within 20 cm of the surface. The relation between DD and soil moisture was very similar to that of DD and GWL (Figures S6 and S4).

In the Cha catchment, the maximum DD was reached very quickly after the start of each rainfall event (Figure 5, Figures S7 and S9). We thus did not observe repetitive rainfall-driven expansion-contraction patterns in Cha (Figure S9) and found a counter-clockwise hysteresis in the DD-q relationship only for two events in the drier period (16th of September and 21st of October; Figure S9).

4 | DISCUSSION

4.1 | Evaluation of the CEASE method

The CEASE method combines high temporal-resolution data from sensors and high spatial-resolution data from surveys to obtain continuous DD time series and flow presence maps. Our analyses show that the CEASE method provides reliable estimates of the short-term changes in DD in both catchments if the survey data represents the range of hydrological conditions of the period of interest (Table 1). The negligible differences in method performance metrics for all tests using different sensor data (Table 1) indicate that at least for the two study catchments, the number and location of sensors have a minor effect on the CEASE method performance. Using only one sensor at the catchment outlet, or the outlet of the larger Erl catchment was already informative (accuracies from 93% to 96%). This is likely due to the synchronicity in the streamflow at the different stream locations (e.g., the R^2 between the discharge measured at the outlet of Erl (E1) and the outlet of Lan and Cha was 0.85 and 0.74, respectively). Previous research reported a high similarity in the discharge regimes between the Alp river and its upstream torrents, one of which is the Erlenbach (Staehli et al., 2021). This finding has important implications as it allows us to reduce the efforts to monitor intermittent streams in these types of catchments. It also allows us to only use water level data from the catchment outlet with the maps of the flowing stream network to derive estimates of the DD. This makes it possible to estimate the variations in the DD based on the historic discharge time series if the stream network has not changed considerably over time, (e.g., due to sediment transport), there have been no changes in the relation between GWLs in the catchment and streamflow (e.g., due to groundwater pumping), or changes in the dominant runoff processes (e.g., due to land use change).

As expected, using only five or fewer surveys in the CEASE method resulted in lower accuracy and sensitivity for both catchments (Figure 5). This highlights the importance of the survey data to reconstruct the short-term DD dynamics. However, for the test performed for three surveys during varying conditions (Table 1), the performance

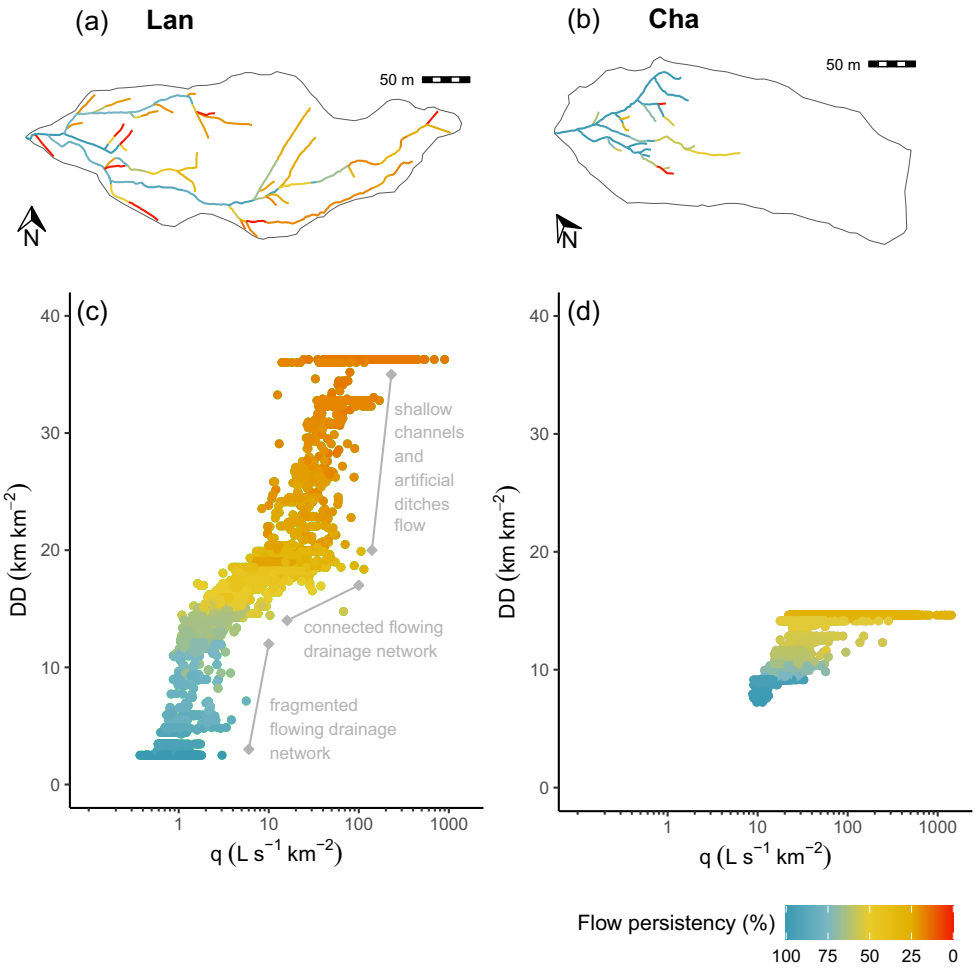

FIGURE 7 Maps of the persistency of flow in Lan (a) and Cha (b) together with the relationship between drainage density and specific discharge in Lan (c) and Cha (d). The channel reaches on the maps (a, b) are colour-coded by the flow persistency, that is, percent of the time each reach was flowing during the study period based on the 10-min resolution CEASE method estimates. The points on the lower panels (c, d) present the hourly data for the entire study period and are colour-coded by the lowest flow persistency (based on panels a, b) from all the channels that were flowing at a given point in time.

metrics were high, suggesting that the method can reliably predict the flow presence if surveys are available for a range of conditions, especially for the Lan catchment. The fact that the test with only dry-condition surveys resulted in biased predictions is not surprising given the hierarchical expansion of the FDN (Botter et al., 2021). Because reaches with low local persistency will only be activated during very wet conditions, a reliable 'flow'/'no-flow' water level threshold T_{ij} can only be found if the surveys capture a correspondingly wide range in hydro-climatic conditions.

In general, our scenario analysis shows that surveys during dry and wet conditions are very informative for establishing T_{ij} thresholds in reaches with high and low flow persistency, respectively. Therefore, we recommend doing surveys during the widest possible range of hydrological conditions to capture most flow states, especially in reaches with very high and very low flow persistency. The considerable difference between the specificity for Lan and Cha for all scenarios (Table 1) suggests that the method tended to overestimate the DD for Cha. This is likely caused by the fact that the summer of 2021 was relatively wet. As a result, many reaches in Cha kept flowing throughout the monitoring period (Figure 7b), leading to an underrepresentation of the 'no-flow' stream state in our dataset, and a less robust estimation of flow states in Cha. In Lan, 57% of all channel reaches had a flow persistency <50% (Figure 7a), whereas this was the case for only 7% of the reaches in Cha (Figure 7b). Thus, the chances for mapping these reaches as 'not flowing' in Cha during dry conditions were very small, contributing to a less certain threshold T_{ij}, and the larger decrease in sensitivity for Lan (−65%) than in Cha (−20%) compared to the best-case scenario.

The CEASE method is based on the threshold behaviour of flow activation, similar to the work of Durighetto and Botter (2022). The existence of repetitive patterns of contraction and expansion for the 27 rainfall events (Figure 8 and Figure S5) suggests that the catchments indeed behave in a predictive way, which potentially allows for the application of the analytical model based on flow persistency of Durighetto and Botter (2022). Unlike the analytical model of Durighetto and Botter (2022), the CEASE method can incorporate data from different water level sensors, which can help to avoid bias related to the use of data from one location (Table 1) and to explore the potential different behaviour during the rising and falling limb of the hydrograph (i.e., hysteresis). The CEASE method is purely empirical and does not use information on upslope contributiong areas or other topographic information to estabilish "flow"/"no-flow" thresholds. This is an advantage when the stream network dynamics are not well related to topography, but rather to geology or human impacts, such as artificial ditches.

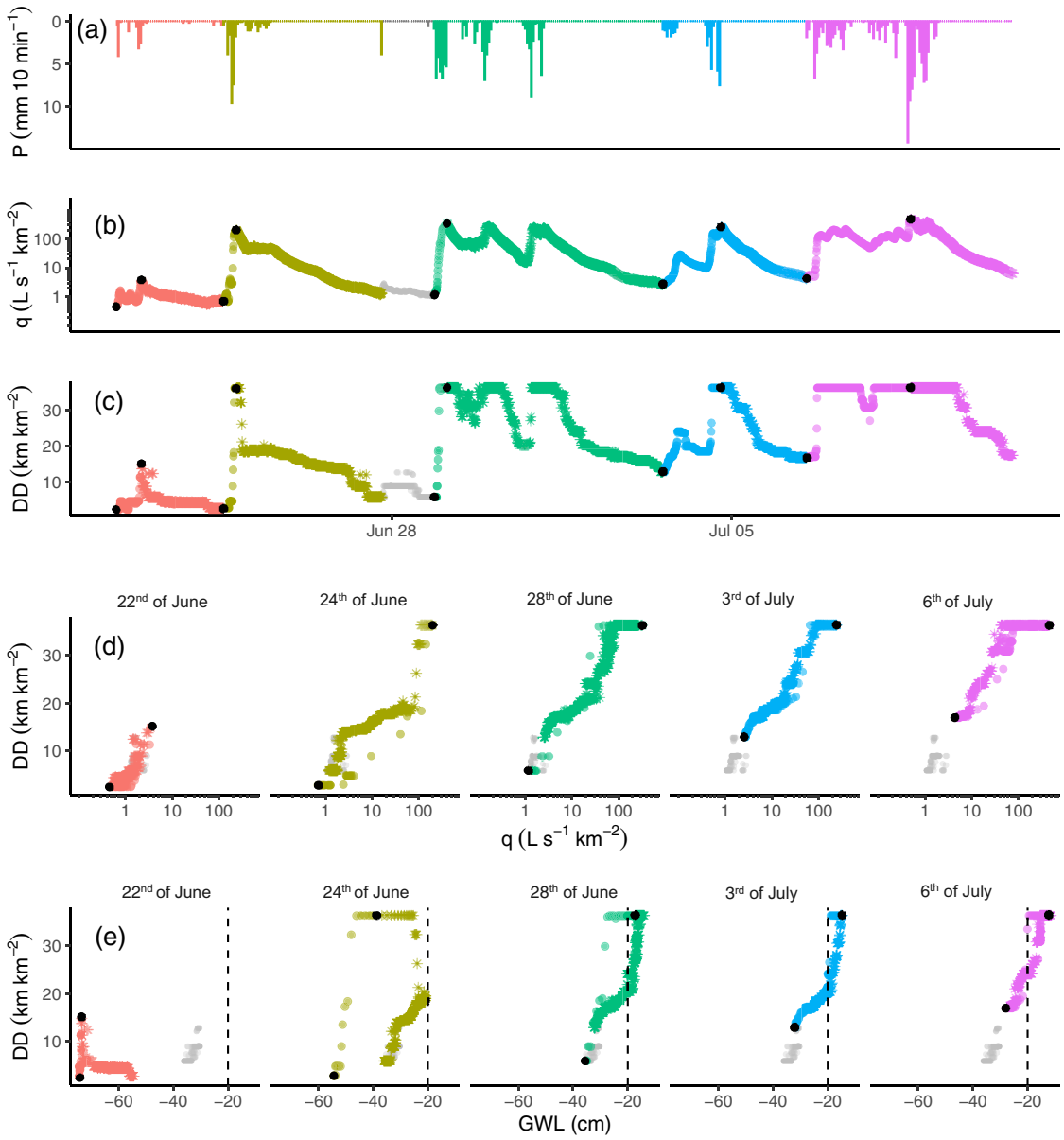

FIGURE 8 Time series of precipitation (a), specific discharge (b) the simulated DD (c) in Lan during five selected rainfall events, and the relationship between DD and specific discharge (d) and the groundwater level at location LGW1 (e). The data are colour-coded by rainfall events, with dots and stars indicating the rising limb and recession phase, respectively; data points during peak discharge are shown in black; non-event data are shown in grey.

The CEASE method can easily be applied to other headwater catchments because it uses only standard hydrometric measurements. The method can be applied to selected parts of the catchment and flow state observations can be made on different days, opening the possibility to apply the method to larger catchments (that cannot be surveyed on 1 day) if enough water level monitoring locations are available to account for the spatial heterogeneity in precipitation and flow responses. Besides that, the method is insensitive to gaps in the water level time series because it combines data from multiple sensors for each timestep. A major limitation of the CEASE method is its requirement for flow presence observations during a range of hydro-climatic conditions. However, our study shows that even if the number of field surveys is reduced to six, the method performance metrics are still high and stable. Although the CEASE method cannot predict DD in un-mapped catchments, it can potentially be used to obtain high-resolution DD time series for catchments for which survey data and high-resolution water level or discharge data are available if the stream network and the relation between groundwater and streamflow have not changed considerably over time (e.g., Godsey & Kirchner, 2014; Jensen et al., 2017; Lovill et al., 2018; Whiting & Godsey, 2016).

4.2 | Differences in DD dynamics between the two catchments

The DDs in both Lan and Cha were in line with those reported in previous studies in the neighbouring Studibach catchment (DD up to 29 km km^{-2}; van Meerveld et al., 2019). They were a few times higher than the DD values reported by Prancevic and Kirchner (2019) for surveys in other catchments, likely because in Erl the climatic conditions are wet and soils are not very permeable.

Despite their proximity, the short-term DD dynamics in the two catchments differed. The DD was more stable over time in Cha, which was already apparent from the field surveys (Figure 3). The variations in DD were much larger for Lan than Cha, even when we scaled the FDN to the total length of all the channels (Figure 4). The differences in DD variations can be explained by the subsurface properties and related topography of the two catchments. Most of the Lan catchment has gentle slopes (Figure 1) but only a relatively small part of the Lan catchment near the outlet has a relatively high (6–9) TWI (Beven & Kirkby, 1979). In the neighbouring Studibach catchment, groundwater tables and dynamics were related to TWI (Rinderer et al., 2017). Thus, the groundwater table near the Lan outlet was likely very shallow, leading to a flow persistency close to or equal to 100% for most of the streams in this area (Figure 7). A similar zone with high TWI values and, thus, water tables are found in the northwest part of the Cha catchment (e.g., Figure S3, location CBGW1), but the streams in this area account for a much larger portion of the total drainage network. The other parts of the Cha catchment are much steeper and do not have a well-developed drainage network, causing an underrepresentation of reaches with low- or mid-range persistency. There are no geomorphic channels in the southeast part of the Cha catchment. This likely reflects deeper infiltration than in the northwest part of the catchment and the deeper groundwater tables (e.g., Figure S3, location CBGW2). In the central part of the catchment where the hillslopes become less steep, there are multiple springs. These springs were active throughout the monitoring period contributing to the low variability in DD in Cha.

The presence of artificial ditches contributes to the large and variable DD in Lan as well. Previous research (Datry et al., 2023; Hammond et al., 2021) has shown that flow ceases earlier in catchments with anthropogenic modifications of the drainage network. As expected, all ditches in Lan had a low flow persistency. In Cha, all stream channels formed naturally where the surface flow pathways are concentrated enough to erode the material. Instead, in Lan additional ditches were created to drain areas where the flow is slower and flow paths are more diverging. As a result, they flow only during or after rainfall events.

4.3 | Inferences about streamflow-generation processes

The short-term q-DD relationship in Lan was not well explained by the power-law relation that was initially proposed by Godsey and Kirchner (2014). Instead, we find a more complex DD-q relationship (Figure 8) than what would have been expected from seasonal survey data (Figure 6; Prancevic & Kirchner, 2019). The S-shaped q-DD relationship in Lan can be explained by two main factors: (1) FDN being fragmented during drier (DDs <15 km km^{-2}, discharge <2 L s^{-1} km^{-2}) and connected during wetter conditions (DDs >15 km km^{-2}, discharge >2 L s^{-1} km^{-2}); (2) multiple shallow (<10 cm incised) channels and artificial ditches with a low specific discharge, that are activated only when conditions are very wet (discharge >11 L s^{-1} km^{-2}), causing the steep q-DD relationship. This is consistent with a previous analysis of flow regimes for 540 catchments in the United States that revealed that in catchments with anthropogenic influences flow ceases earlier and the duration of the dry-down period is shorter (Hammond et al., 2021). Furthermore, the slope of the q-DD relationship during the recession for Lan depended on the antecedent wetness conditions (Figure 8 and Figure S5). During wet conditions, the DD stays at its full extent longer likely because the rising GWLs maintain water flow in the channels. However, when the catchment starts to dry and GWL drops, the DD decreases rapidly due to the deactivation of flow in the less incised streams and the ditches.

Figure 8 indicates furthermore that the antecedent wetness conditions can play an important role in the timing of FDN expansion during rainfall events, which is consistent with the findings of Jensen et al. (2019). The first rainfall events after dry periods are characterized by a slower increase in DD, but once the catchment is wet, the responses are synchronous. Jensen et al. (2019) also reported hysteresis for the wet portion of the channel network during dry antecedent conditions, and a lack of hysteresis when conditions were wet. They linked it to an insufficient increase in the deep groundwater table to maintain flow in the channels after an event. However, contrary to their results, the hysteresis loop for the study catchments was counterclockwise after dry periods. This is likely caused by several processes. At the beginning of the event, most flowing channels occur in the lowest part of the catchment, which is characterized by shallow GWLs (Figure 7a). Direct rainfall runoff in wet channels, as well as a rapid increase of GWL due to infiltrating rainwater (cf., Rinderer et al., 2016) causes a quick streamflow response. Because the reaches in this part of the catchment are already flowing (as indicated by their high flow persistency; Figure 7a), discharge increases faster than DD. The lower DD on the rising hydrograph limb can also be caused by the higher infiltration and seepage losses along the dry reaches (Batlle-Aguilar & Cook, 2012; Niswonger et al., 2008). Transient infiltration rates along the dry channels at the event onset can be up to three orders of magnitude higher than during steady-state conditions (Blasch et al., 2006). With ongoing rainfall, the infiltration rates decrease (Batlle-Aguilar & Cook, 2012; Blasch et al., 2006), causing more reaches of the channel network to connect. With continued increases in the GWL, surface flow emerges in the upstream tributaries, causing a rapid increase in DD. At the end of a rainfall event, streamflow at the outlet recedes faster than DD. The rising GWL and continued seepage at the channel heads maintain a high DD, even though the groundwater discharge is small and decreasing, resulting in less streamflow at the outlet.

For rainfall events following wet antecedent conditions, DD and discharge respond synchronously (i.e., no hysteresis) in Lan. With wetter conditions, the infiltration rates into the dry streambeds are lower (Batlle-Aguilar & Cook, 2012; Blasch et al., 2006), catchment subsurface storage is higher, and the maximum subsurface transport capacity is exceeded faster. Therefore, streamflow emerges earlier in multiple reaches with a low flow persistency. Moreover, we observed a rapid increase in DD with wetter conditions when the GWL rose to within 20 cm below the surface and streamflow was initiated in multiple shallow-incised channels and artificial ditches (Figures 7 and 8). The Gleysols of the study sites (Schleppi et al., 1998) are characterized by low drainable porosity and low hydraulic conductivity. When the GWL rise into the higher permeability topsoil (i.e., within 20 cm), water is quickly transported to the stream, leading to both a larger increase in discharge and DD.

In Cha, the q-DD relationship was less complex than in Lan and, except at high flows, could be described by a single power-law curve. Hysteresis was observed only for one event following dry antecedent conditions (Figure S9). In comparison to other years, June and July 2021 were very wet. It is possible, that the DD dynamics in Cha are more complex during drier years. Five out of 15 channel heads in the central part of the catchment (Figure 7b) are groundwater springs that were active throughout the monitoring period, resulting in a relatively high DD with low variability. Most of the DD variations were caused by two channels located above the groundwater springs in the steeper, southeast part of the catchment. These channels have a lower TWI, and deeper GWL (Figure S3). The area without a channel network in Cha is much larger than in Lan, and thus, deep infiltration and delayed groundwater discharge are likely to dominate in a large part of Cha.

5 | CONCLUSIONS

The CEASE method combines high temporal resolution water level data with high spatial resolution mapping surveys of the flow state for the entire stream network to determine the variation in the flowing stream DD during rainfall events. For the two studied headwater catchments, it is best to use at least six field surveys during varying hydrological conditions to adequately represent the reaches with high and low flow persistency. The number and location of the water level sensors had only a small effect on the performance of the method and even the use of just the time series from the sensor at the catchment outlet yielded high-accuracy results. The method can be applied in different catchments contributing to the availability of data on short-term FDNs.

The more variable DD in Lan than Cha can be explained by the differences in subsurface properties and related topography. The relation between DD and specific discharge did not strictly follow a power-law relationship; the shape of the relation could be explained by the topography of the different parts of the catchment and the reaches that started to flow at different catchment wetness conditions. Furthermore, the event scale DD-specific discharge relation was hysteretic when the antecedent conditions were dry. The relation between DD and the GWL, similarly, depended on the antecedent conditions. The observations agree with previous studies that found a relation between flow persistency and topographic metrics, such as elevation, slope, and TWI (e.g., Warix et al., 2021). Future studies should investigate FDNs and their short-term dynamics, as well as the performance of the CEASE method, in catchments with different characteristics.

ACKNOWLEDGEMENTS

We thank Barbara Strobl, Joshua Haas, Nina Nagel, Rick Assendelft, Florian Käslin, Pascal Arpagaus, Florian Lustenberger, Alex Karapanscev, Kari Steiner, Wojciech Ozga, Stefan Boss, and Alpwirtschaf Furggelen for helping with equipment installation and maintenance, and data collection. We also thank Marius Luder for his help in data collection and processing. We are grateful to James W. Kirchner for stimulating discussions and Sara R. Warix and two other anonymous reviewers for their helpful comments that improved this manuscript. This project was funded by the Swiss National Science Foundation (grant PR00P2_185931).

DATA AVAILABILITY STATEMENT

Hydrological data from this study is available on EnviDat (Bujak-Ozga et al., 2023). The CEASE method source code is available on Zenodo (Bujak-Ozga, 2023b).

ORCID

Izabela Bujak-Ozga https://orcid.org/0000-0002-3059-7376
H.J. (Ilja) van Meerveld https://orcid.org/0000-0002-7547-3270
Andrea Rinaldo https://orcid.org/0000-0002-2546-9548
Jana von Freyberg https://orcid.org/0000-0002-2111-0001

REFERENCES

Acuña, V., Datry, T., Marshall, J., Barceló, D., Dahm, C. N., Ginebreda, A., & Palmer, M. A. (2014). Why should we care about temporary waterways? *Science*, *343*(6175), 1080–1081.

Aho, K., Kriloff, C., Godsey, S. E., Ramos, R., Wheeler, C., You, Y., & Kuehn, K. A. (2023). Non-perennial stream networks as directed acyclic graphs: The R-package streamDAG. *Environmental Modelling & Software*, *167*, 105775.

Assendelft, R. S., & van Meerveld, H. I. (2019). A low-cost, multi-sensor system to monitor temporary stream dynamics in mountainous headwater catchments. *Sensors*, *19*(21), 4645.

Batlle-Aguilar, J., & Cook, P. G. (2012). Transient infiltration from ephemeral streams: A field experiment at the reach scale. *Water Resources Research*, *48*(11), W11518. https://doi.org/10.1029/2012WR012009

Bertassello, L. E., Durighetto, N., & Botter, G. (2022). Eco-hydrological modelling of channel network dynamics—Part 2: Application to metapopulation dynamics. *Royal Society Open Science*, *9*(11), 220945.

Beven, K. J., & Kirkby, M. J. (1979). A physically based, variable contributing area model of basin hydrology/Un modèle à base physique de zone d'appel variable de l'hydrologie du bassin versant. *Hydrological Sciences Journal*, *24*(1), 43–69.

Blasch, K. W., Ferre, T. P., Hoffmann, J. P., & Fleming, J. B. (2006). Relative contributions of transient and steady state infiltration during ephemeral streamflow. *Water Resources Research*, *42*(8), 1–13.

Botter, G., Vingiani, F., Senatore, A., Jensen, C., Weiler, M., McGuire, K., & Durighetto, N. (2021). Hierarchical climate-driven dynamics of the

active channel length in temporary streams. *Scientific Reports*, *11*(1), 21503.

Bujak-Ozga, I. (2023a). *TempAqua app iOS for intermittent streams mapping (v2.3.1)*. Zenodo. https://doi.org/10.5281/zenodo.10035289

Bujak-Ozga, I. (2023b). *ConsEnsuAI state estimation method (CEASE): v0.8 (v0.8)*. Zenodo. https://doi.org/10.5281/zenodo.10035126

Bujak-Ozga, I., van Meerveld, I., Rinaldo, A., & von Freyberg, J. (2023). *Short-term drainage density dynamics dataset*. EnviDat. https://doi.org/10.16904/envidat.450

Costigan, K. H., Jaeger, K. L., Goss, C. W., Fritz, K. M., & Goebel, P. C. (2016). Understanding controls on flow permanence in intermittent rivers to aid ecological research: Integrating meteorology, geology and land cover. *Ecohydrology*, *9*(7), 1141–1153.

Datry, T., Truchy, A., Olden, J. D., Busch, M. H., Stubbington, R., Dodds, W. K., & Allen, D. (2023). Causes, responses, and implications of anthropogenic versus natural flow intermittence in river networks. *Bioscience*, *73*(1), 9–22.

Dodds, W. K., Gido, K., Whiles, M. R., Fritz, K. M., & Matthews, W. J. (2004). Life on the edge: The ecology of Great Plains prairie streams. *Bioscience*, *54*(3), 205–216.

Durighetto, N., Bertassello, L. E., & Botter, G. (2022). Eco-hydrological modelling of channel network dynamics—Part 1: Stochastic simulation of active stream expansion and retraction. *Royal Society Open Science*, *9*(11), 220944.

Durighetto, N., & Botter, G. (2022). On the relation between active network length and catchment discharge. *Geophysical Research Letters*, *49*(14), e2022GL099500.

Durighetto, N., Mariotto, V., Zanetti, F., McGuire, K. J., Mendicino, G., Senatore, A., & Botter, G. (2022). Probabilistic description of streamflow and active length regimes in rivers. *Water Resources Research*, *58*(4), e2021WR031344.

Durighetto, N., Vingiani, F., Bertassello, L. E., Camporese, M., & Botter, G. (2020). Intraseasonal drainage network dynamics in a headwater catchment of the Italian Alps. *Water Resources Research*, *56*(4), e2019WR025563.

Fritz, K. M., Hagenbuch, E., D'Amico, E., Reif, M., Wigington, P. J., Jr., Leibowitz, S. G., & Nadeau, T. L. (2013). Comparing the extent and permanence of headwater streams from two field surveys to values from hydrographic databases and maps. *JAWRA Journal of the American Water Resources Association*, *49*(4), 867–882.

Giezendanner, J., Benettin, P., Durighetto, N., Botter, G., & Rinaldo, A. (2021). A note on the role of seasonal expansions and contractions of the flowing fluvial network on metapopulation persistence. *Water Resources Research*, *57*(11), e2021WR029813.

Godsey, S. E., & Kirchner, J. W. (2014). Dynamic, discontinuous stream networks: Hydrologically driven variations in active drainage density, flowing channels and stream order. *Hydrological Processes*, *28*(23), 5791–5803.

González-Ferreras, A. M., & Barquín, J. (2017). Mapping the temporary and perennial character of whole river networks. *Water Resources Research*, *53*(8), 6709–6724.

Gregory, K. J., & Walling, D. E. (1968). The variation of drainage density within a catchment. *Hydrological Sciences Journal*, *13*(2), 61–68.

Hale, R. L., & Godsey, S. E. (2019). Dynamic stream network intermittence explains emergent dissolved organic carbon chemostasis in headwaters. *Hydrological Processes*, *33*(13), 1926–1936.

Hammond, J. C., Zimmer, M., Shanafield, M., Kaiser, K., Godsey, S. E., Mims, M. C., Zipper, S. C., Burrows, R. M., Kampf, S. K., Dodds, W., Jones, C. N., Krabbenhoft, C. A., Boersma, K. S., Datry, T., Olden, J. D., Allen, G. H., Price, A. N., Costigan, K., Hale, R., … Allen, D. C. (2021). Spatial patterns and drivers of nonperennial flow regimes in the contiguous United States. *Geophysical Research Letters*, *48*(2), e2020GL090794. https://doi.org/10.1029/2020GL090794

Hanski, I., & Ovaskainen, O. (2000). The metapopulation capacity of a fragmented landscape. *Nature*, *404*(6779), 755–758.

Hantke, R., Trümpy, R., BAumeler, A., Bollinger, D., Felber, P., Letsch, D., & Grünig, A. (2022). Blatt 1152 Ibergeregg—Geologischer Atlas der Schweiz 1: 25 000, Karte 175.

Ho, T. K. (1995). Random Decision Forest. *Proceedings of the 3rd International Conference on Document Analysis and Recognition* (pp. 278–282).

Horton, R. E. (1932). Drainage-basin characteristics. *Transactions, American Geophysical Union*, *13*(1), 350–361.

Jaeger, K. L., & Olden, J. D. (2012). Electrical resistance sensor arrays as a means to quantify longitudinal connectivity of rivers. *River Research and Applications*, *28*(10), 1843–1852.

Jensen, C. K., McGuire, K. J., McLaughlin, D. L., & Scott, D. T. (2019). Quantifying spatiotemporal variation in headwater stream length using flow intermittency sensors. *Environmental Monitoring and Assessment*, *191*, 226. https://doi.org/10.1007/s10661-019-7373-8

Jensen, C. K., McGuire, K. J., & Prince, P. S. (2017). Headwater stream length dynamics across four physiographic provinces of the Appalachian highlands. *Hydrological Processes*, *31*(19), 3350–3363.

Kaplan, N. H., Sohrt, E., Blume, T., & Weiler, M. (2019). Monitoring ephemeral, intermittent and perennial streamflow: A dataset from 182 sites in the Attert catchment, Luxembourg. *Earth System Science Data*, *11*(3), 1363–1374.

Kulin, G., & Compton, P. R. (1975). *A guide to methods and standards for the measurement of water flow* (Vol. 13). US Department of Commerce, National Bureau of Standards.

Lovill, S. M., Hahm, W. J., & Dietrich, W. E. (2018). Drainage from the critical zone: Lithologic controls on the persistence and spatial extent of wetted channels during the summer dry season. *Water Resources Research*, *54*, 5702–5726. https://doi.org/10.1029/2017WR021903

Mahoney, D. T., Christensen, J. R., Golden, H. E., Lane, C. R., Evenson, G. R., White, E., & Agouridis, C. T. (2023). Dynamics of streamflow permanence in a headwater network: Insights from catchment-scale model simulations. *Journal of Hydrology*, *620*, 129422.

Mari, L., Casagrandi, R., Bertuzzo, E., Rinaldo, A., & Gatto, M. (2014). Metapopulation persistence and species spread in river networks. *Ecology Letters*, *17*(4), 426–434.

Messager, M. L., Lehner, B., Cockburn, C., Lamouroux, N., Pella, H., Snelder, T., Tockner, K., Trautmann, T., Watt, C., & Datry, T. (2021). Global prevalence of non-perennial rivers and streams. *Nature*, *594*, 391–397. https://doi.org/10.1038/s41586-021-03565-5

Meyer, J. L., Strayer, D. L., Wallace, J. B., Eggert, S. L., Helfman, G. S., & Leonard, N. E. (2007). The contribution of headwater streams to biodiversity in river networks 1. *JAWRA Journal of the American Water Resources Association*, *43*(1), 86–103.

Nikolaidis, N. P., Demetropoulou, L., Froebrich, J., Jacobs, C., Gallart, F., Prat, N., & Perrin, J. L. (2013). Towards sustainable management of Mediterranean river basins: Policy recommendations on management aspects of temporary streams. *Water Policy*, *15*(5), 830–849.

Niswonger, R. G., Prudic, D. E., Fogg, G. E., Stonestrom, D. A., & Buckland, E. M. (2008). Method for estimating spatially variable seepage loss and hydraulic conductivity in intermittent and ephemeral streams. *Water Resources Research*, *44*(5), 1–14.

Prancevic, J. P., & Kirchner, J. W. (2019). Topographic controls on the extension and retraction of flowing streams. *Geophysical Research Letters*, *46*(4), 2084–2092.

R Core Team. (2022). *R: A language and environment for statistical computing*. R Foundation for Statistical Computing https://www.R-project.org/

Rinaldo, A., Gatto, M., & Rodriguez-Iturbe, I. (2018). River networks as ecological corridors: A coherent ecohydrological perspective. *Advances in Water Resources*, *112*, 27–58.

Rinderer, M., McGlynn, B. L., & Van Meerveld, H. J. (2017). Groundwater similarity across a watershed derived from time-warped and flow-corrected time series. *Water Resources Research*, *53*(5), 3921–3940.

Rinderer, M., van Meerveld, H. J., & Seibert, J. (2014). Topographic controls on shallow groundwater levels in a steep, pre-alpine catchment:

When are the TWI assumptions valid? *Water Resources Research*, *50*(7), 6067–6080.
Rinderer, M., van Meerveld, I., Stähli, M., & Seibert, J. (2016). Is groundwater response timing in a pre-alpine catchment controlled more by topography or by rainfall? *Hydrological Processes*, *30*(7), 1036–1051.
Schleppi, P., Muller, N., Feyen, H., Papritz, A., Bucher, J. B., & Flühler, H. (1998). Nitrogen budgets of two small experimental forested catchments at Alptal, Switzerland. *Forest Ecology and Management*, *101*(1–3), 177–185.
Senatore, A., Micieli, M., Liotti, A., Durighetto, N., Mendicino, G., & Botter, G. (2021). Monitoring and modeling drainage network contraction and dry down in Mediterranean headwater catchments. *Water Resources Research*, *57*(6), e2020WR028741.
Shanafield, M., Bourke, S. A., Zimmer, M. A., & Costigan, K. H. (2021). An overview of the hydrology of non-perennial rivers and streams. *Wiley Interdisciplinary Reviews: Water*, *8*(2), e1504.
Staehli, M., Seibert, J., Kirchner, J. W., von Freyberg, J., & van Meerveld, I. (2021). Hydrological trends and the evolution of catchment research in the Alptal valley, Central Switzerland. *Hydrological Processes*, *35*, e14113. https://doi.org/10.1002/hyp.14113
Stubbington, R., Acreman, M., Acuña, V., Boon, P. J., Boulton, A. J., England, J., & Wood, P. J. (2020). Ecosystem services of temporary streams differ between wet and dry phases in regions with contrasting climates and economies. *People and Nature*, *2*(3), 660–677.
Stubbington, R., England, J., Wood, P. J., & Sefton, C. E. (2017). Temporary streams in temperate zones: Recognizing, monitoring, and restoring transitional aquatic-terrestrial ecosystems. *Wiley Interdisciplinary Reviews: Water*, *4*(4), e1223.
SwissTopo - Federal Office of Topography swisstopo. (2019). 0.5 m resolution digital elevation model swissALTI3D.
van Meerveld, H. I., Sauquet, E., Gallart, F., Sefton, C., Seibert, J., & Bishop, K. (2020). Aqua temporaria incognita. *Hydrological Processes*, *34*(26), 5704–5711.
van Meerveld, H. J., Kirchner, J. W., Vis, M. J., Assendelft, R. S., & Seibert, J. (2019). Expansion and contraction of the flowing stream network alter hillslope flowpath lengths and the shape of the travel time distribution. *Hydrology and Earth System Sciences*, *23*(11), 4825–4834.
von Freyberg, J., Rucker, A., Zappa, M., Schlumpf, A., Studer, B., & Kirchner, J. W. (2022). Four years of daily stable water isotope data in stream water and precipitation from three Swiss catchments. *Scientific Data*, *9*, 46. https://doi.org/10.1038/s41597-022-01148-1
von Schiller, D., Bernal, S., Dahm, C. N., & Martí, E. (2017). Nutrient and organic matter dynamics in intermittent rivers and ephemeral streams. In Datry, T., Bonada, N., & Boulton, A. *Intermittent rivers and ephemeral streams* (pp. 135–160). Academic Press.
Ward, A. S., Schmadel, N. M., & Wondzell, S. M. (2018). Simulation of dynamic expansion, contraction, and connectivity in a mountain stream network. *Advances in Water Resources*, *114*, 64–82.
Warix, S. R., Godsey, S. E., Lohse, K. A., & Hale, R. L. (2021). Influence of groundwater and topography on stream drying in semi-arid headwater streams. *Hydrological Processes*, *35*(5), e14185.
Whiting, J. A., & Godsey, S. E. (2016). Discontinuous headwater stream networks with stable flowheads, Salmon River basin, Idaho. *Hydrological Processes*, *30*, 2305–2316. https://doi.org/10.1002/hyp.10790
Zanetti, F., Durighetto, N., Vingiani, F., & Botter, G. (2022). Analyzing river network dynamics and the active length–discharge relationship using water presence sensors. *Hydrology and Earth System Sciences*, *26*(13), 3497–3516.
Zimmer, M. A., Burgin, A. J., Kaiser, K., & Hosen, J. (2022). The unknown biogeochemical impacts of drying rivers and streams. *Nature Communications*, *13*, 7213. https://doi.org/10.1038/s41467-022-34903-4
Zimmer, M. A., & McGlynn, B. L. (2017a). Time-lapse animation of hillslope groundwater dynamics details event-based and seasonal bidirectional stream-groundwater gradients. *Hydrological Processes*, *35*(10), 1983-1985. https://doi.org/10.1002/hyp.11124
Zimmer, M. A., & McGlynn, B. L. (2017b). Bidirectional stream–groundwater flow in response to ephemeral and intermittent streamflow and groundwater seasonality. *Hydrological Processes*, *31*(22), 3871–3880.
Zimmer, M. A., & McGlynn, B. L. (2017c). Ephemeral and intermittent runoff generation processes in a low relief, highly weathered catchment. *Water Resources Research*, *53*(8), 7055–7077.

SUPPORTING INFORMATION

Additional supporting information can be found online in the Supporting Information section at the end of this article.

How to cite this article: Bujak-Ozga, I., van Meerveld, H. J. (I.), Rinaldo, A., & von Freyberg, J. (2023). Short-term dynamics of drainage density based on a combination of channel flow state surveys and water level measurements. *Hydrological Processes*, *37*(12), e15041. https://doi.org/10.1002/hyp.15041